NASA TECHNICAL NOTE

NASA TN D-5784

NASA TN D-5784

CHARACTERIZATION AND DESIGN MECHANICS FOR FIBER-REINFORCED METALS

by Christos C. Chamis

Lewis Research Center

Cleveland, Ohio 44135

NATIONAL AERONAUTICS AND SPACE ADMINISTRATION • WASHINGTON, D. C. • MAY 1970

1. Report No. NASA TN D-5784	2. Government Accession No.	3. Recipient's Catalog No.
4. Title and Subtitle CHARACTERIZATION AND DESIGN MECHANICS FOR FIBER-REINFORCED METALS		5. Report Date May 1970
		6. Performing Organization Code
7. Author(s) Christos C. Chamis		8. Performing Organization Report No. E-5364
9. Performing Organization Name and Address Lewis Research Center National Aeronautics and Space Administration Cleveland, Ohio 44135		10. Work Unit No. 129-03
		11. Contract or Grant No.
		13. Type of Report and Period Covered
12. Sponsoring Agency Name and Address National Aeronautics and Space Administration Washington, D.C. 20546		Technical Note
		14. Sponsoring Agency Code

15. Supplementary Notes

16. Abstract

Certain aspects of fiber composite mechanics are utilized to characterize fiber-reinforced metals in the elastic range of the fiber when the properties of their constituents are available and the fabrication processes are known. The concept is illustrated by selecting a boron aluminum unidirectional fiber composite system. This system is characterized from the geometry, thermoelastic response, and strength behavior viewpoints. Some comparisons with limited experimental data are made for correlation purposes. Theoretical results of the boron aluminum composite are presented to illustrate the trends in the thermoelastic and strength properties and to point out difficulties in experimental work and design. The detrimental effects of voids (porosity) on some of these properties are also illustrated. Results are presented as a design aid and areas for additional experimental work and research are identified. Additional results are presented which provide better insight to metallic composite structural behavior.

17. Key Words (Suggested by Author(s)) Fiber composites; metallic matrix; composite mechanics; composite characterization; thermal properties; elastic properties; strength properties; combined stress strength; off-axis strength; delamination parameter; buckling parameter	18. Distribution Statement Unclassified – unlimited		
19. Security Classif. (of this report) Unclassified	20. Security Classif. (of this page) Unclassified	21. No. of Pages 45	22. Price* $3.00

*For sale by the Clearinghouse for Federal Scientific and Technical Information
Springfield, Virginia 22151

CHARACTERIZATION AND DESIGN MECHANICS FOR

FIBER-REINFORCED METALS

by Christos C. Chamis

Lewis Research Center

SUMMARY

Certain aspects of fiber composite mechanics are utilized to characterize fiber-reinforced metals in the elastic range of the fiber when the properties of their constituents are available and the fabrication processes are known. The concept is illustrated by selecting a boron aluminum unidirectional fiber composite system. This system is characterized from the geometry, thermoelastic response, and strength behavior viewpoints. Some comparisons with limited experimental data are made for correlation purposes. Theoretical results of the boron aluminum composite are presented to illustrate the trends in the thermoelastic and strength properties and to point out difficulties in experimental work and design. The detrimental effects of voids (porosity) on some of these properties are also illustrated. Failure envelopes for combined stress and off-axis loading are constructed as an aid to designers. Some results for angle-ply composites are presented. References dealing with other aspects of composite mechanics, not covered herein, are cited. Other design factors such as ply thickness, density, delamination, and buckling parameters are discussed, and design curves for these factors are plotted.

The composite mechanics proposed herein provides a useful tool for the complete linear characterization and generation of design data of fiber-reinforced metals. Areas are pointed out where additional experimental data and further research are needed.

INTRODUCTION

The technology of fiber-reinforced metals has advanced to the point where actual hardware components are being fabricated from these materials. References 1 to 5 provide a thorough review of the state-of-the-art of fiber-reinforced metals. Several of their underlying principles, their various fabrication processes, and some of their peculiarities are described in these references. Some systems that have been success-

fully fabricated and hold promise for structural components are carbon-filament-reinforced cobalt and nickel (ref. 6), beryllium-fiber-reinforced aluminum (ref. 7), refractory-fiber-reinforced superalloys (refs. 8 and 9), boron-fiber-reinforced titanium (ref. 10), graphite-fiber-reinforced nickel (ref. 11), and boron-fiber-reinforced aluminum (ref. 12). Studies on the compatibility of fibers with metal matrices are reported in reference 13. The joining of metallic matrix composites is described in reference 14. One specific application of composites to blading for gas turbine engines is illustrated in reference 15. Additional references on fabrication processes are cited in reference 3.

The available work to date is significant in many respects and has resulted in the accomplishment of several research objectives such as determination of several possible composite systems, demonstration of several possible fabrication processes, and resolution of constituent compatibility, elementary mechanics, and experiments for constituent load transfer. The experimental and theoretical work which leads to efficient component design from fiber-reinforced metals is still in its infant stage. Herein, an important portion of the theoretical aspect of the information domain is treated. The theoretical treatment is supplemented with recommendations on experimental and additional theoretical work which will help complete the major part of this domain.

The theoretical portion of the information domain contains theories for structural and stress analysis, representative macro- and micromechanics, mathematical models, and efficient optimization algorithms. Structural and stress analysis and optimum design of fiber composites, in general, require knowledge of several thermoelastic and strength properties and certain other design factors. Composite properties depend strongly on the quantities of constituent materials present and the angle between the loading and the fiber directions. The large number of possible constituent combinations and fiber orientations in a composite make it considerably difficult, if not impossible, to determine experimentally the thermoelastic and strength properties required in design and analysis. The other alternative is to construct micromechanics theories (ref. 16) to predict several or all of these properties for unidirectional fiber composites (UFC or plies) (fig. 1). Then lamination theory can be used for composite properties in general. The thermoelastic and strength behavior of unidirectional composites is influenced by several factors, some of which are quite difficult to incorporate in mathematical models (ref. 16). Most of these difficulties are bypassed by developing semiempirical theories.

The semiempirical theories proposed in references 17 and 18 have been successfully applied in predicting all the thermoelastic and strength properties of fiber, nonmetallic-matrix composites which exhibit linear behavior. Herein, these theories are applied to predict all of the thermoelastic and strength properties of fiber, metallic-matrix composites in the linear fiber regime.
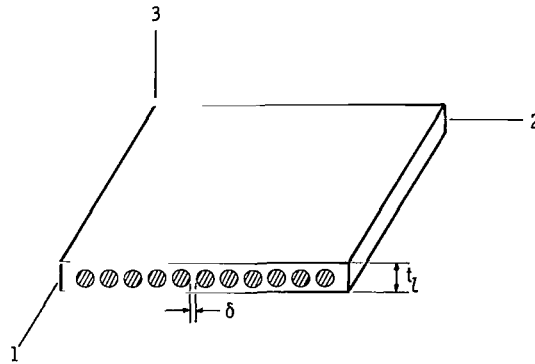
Figure 1. - Boron aluminum ply geometry.

The parameters necessary to describe completely the thermoelastic and strength behavior of unidirectional fiber composites (fig. 1) consist of seven thermal properties (three thermal coefficients of expansion, three conductivities, and one heat capacity), nine elastic properties (three normal or extensional moduli, three shear moduli, and three Poisson ratios), five uniaxial strengths (longitudinal tensile, longitudinal compressive, transverse tensile, transverse compressive, and intralaminar shear), and also a combined stress strength criterion. In addition, factors such as ply thickness, inter-fiber spacing, density, ply weight per unit area, transverse shear delamination crite-rion, buckling coefficients, and weight considerations are important in practical design and tradeoff studies.

The semiempirical theories described in references 17 and 18 are applied to some available experimental results (refs. 19 and 20) to illustrate their application and ver-satility. Subsequently, these theories are employed to predict the complete thermoelas-tic and strength behavior of boron-fiber - aluminum-matrix unidirectional composites. Some typical thermoelastic properties of off-axis and angle-ply composites are shown as a guide to design. Failure envelopes under off-axis loadings and under combined stress are presented. The effects of varying the transverse tensile strength and the intra-laminar shear strength on off-axis failure envelopes are investigated. The methods de-scribed in reference 21 are employed to predict some of the other important design fac-tors mentioned previously (such as transverse shear delamination criterion and buckling coefficient). The results are presented in graphical form.

The final form of the equations used to generate the results is given in the appen-dixes. The physical considerations, assumptions, and detailed derivations are omitted here since they are available in the references cited. The experimental results of ref-ence 22 were used to evaluate some of the correlation coefficients in the semiempirical theories.

The majority of the results presented herein are theoretical, and they were obtained assuming linear or approximately linear UFC behavior to failure. These results show

3

the application of composite mechanics in the characterization and generation of design data for fiber-reinforced metals. In addition, they bring into focus the type of information needed in design, the areas of difficulty in obtaining this information, the experimental data which are still needed, and the possible areas of immediate and future research. The discussion is supplemented by pertinent references in all cases. To this end, the detailed discussion of one specific composite system is sufficient.

SYMBOLS

$A, \bar{A}$	constants, eqs. (A14) and (B5)
a, a_1, a_2	plate dimension; constants, eq. (B8)
B	constant, eq. (A14)
C_f, C_m	constants, eq. (A15)
$\tilde{C}_f, \tilde{C}_m$	constants, eq. (A16)
C_f', C_m'	constants, eq. (A20)
C_f'', C_m''	constants, eq. (A21)
d	diameter
E	normal modulus, or elastic coefficients, or matrix elements
F	failure criterion function
f	functional
G	shear modulus
H_c	heat capacity
$K, \bar{K}$	bulk modulus or heat conductivity
$K_{l\,12}, K_{l\,12}'$	elastic and correlation coefficients, respectively, eq. (B12)
$k, \bar{k}$	apparent and actual volume ratio, respectively
N_f, N_l	number of fibers per end and number of layers, respectively
P_{cr}	buckling load
p	parameter, eq. (B4)
R	transformation matrix, eq. (B18)
S	simple strength, failure or limit stress
ΔT	temperature change

t	thickness
W	weight
x, y, z	structural (load) axes and coordinates thereof
1, 2, 3	material axes (1 axis coincides with fiber direction)
α	thermal coefficient of expansion
$\beta, \tilde{\beta}, \beta', \beta''$	correlation coefficients for ply thermoelastic properties, eqs. (A15), (A16), (A20), and (A21), respectively
$\beta_{kv}, \beta_{k1}, \beta_{k2}, \beta_{k3}$	correlation coefficients for heat conductivities, eqs. (A27) and (A28)
$\beta_{fT, fC, mT, mC, 22T, 22C, 12S}$	correlation coefficients for strength, eqs. (B7) to (B11), respectively
β_t	in situ end, or strand, or yarn, packing array parameter, eq. (A4), fig. 18
δ	interfiber spacing (not center to center), eq. (A3), fig. 19
ϵ	strain
ζ	buckling parameter, fig. 22
θ	angle between load and filament direction
λ_w, λ_s	buckling and delamination parameters, figs. 23 and 24, respectively
ν	Poisson ratio
ρ	weight density
σ	stress
φ_μ	strain magnification factor
{ }	1 column array
[ ]	array
[ ]^T	array transpose
[ ]$^{-1}$	array inverse
Subscripts:	
B	interface bonding
C	compression

c	composite property
D	debonding
f	filament property
i	ply index
l	ply property
m	matrix property
p	limiting property
R	residual stress
S	shear
T	tension
v	void
x, y, z	structural (load) axes direction
1, 2, 3	material axes directions (1 axis coincides with the fiber direction)
α, β	T or C, tension or compression

BRIEF REVIEW OF PHILOSOPHY OF SEMIEMPIRICAL THEORIES

The fundamental concept underlying semiempirical theories is summarized in the next three sentences. A simply mathematical model is selected which is mechanistically representative of the physical state of affairs. The model is rendered predictively correct by strategically incorporated theory-experiment correlation factors. The correlation coefficients are then selected from a composite with some fiber content and made from a particular fabrication process. Subsequently, the theory is used to predict properties of composites of other fiber contents but the same fabrication process. The following example illustrates the concept.

The failure stress of a unidirectional fiber composite takes the following functional form:

$$S_l = f\left[(k, d, N, A)_{f, v}, k_m, (E, \nu, G, S, \epsilon_p)_{f, m}, S_B, \sigma_R, \sigma\right] \tag{1}$$

where S denotes failure or limit stress, k, d, N, and A represent volume ratio, filament diameter, number of fibers per end, and array packing, respectively, E, ν, G, and ϵ_p are the normal modulus, Poisson ratio, shear modulus, and limit strain, respectively; σ denotes stress state due to applied load; the subscripts l, f, v, m, B,

and R denote ply, fiber, void, matrix, bond strength, and residual stress, respectively. Conversion of equation (1) into an explicit form, if possible, would require complex statistical mathematical formalisms. On the other hand, the ply longitudinal tensile failure stress $S_{\ell 11T}$ (fig. 1) can be expressed simply by using a rule-of-mixtures model (eq. (B7), appendix B):

$$S_{\ell 11T} = S_{fT}\left(\beta_{fT}\bar{k}_f + \beta_{mT}\bar{k}_m \frac{E_{m11}}{E_{f11}}\right) \tag{2}$$

where the barred quantities indicate actual volume content, and β_{fT} and β_{mT} are the experiment-theory correlation factors which convert equation (1) to (2). The parameters β_{fT} and β_{mT} embody all the variables which appear in equation (1) but are absent from equation (2). Another way to think of these parameters is as fabrication process variables. Variables such as k_v, A, S_B, and σ_R are associated with a particular fabrication process. As a result, the correlation factors have to be evaluated for some particular composite system for each fabrication process (refs. 17 and 18). Subsequent application of the theories will illustrate evaluation of the theory-experiment correlation factors.

The semiempirical theory described herein will handle composites exhibiting linear or approximate linear behavior. Composites containing ductile fibers exhibit some nonlinear stress-strain behavior. The strength properties of these composites can be predicted by the semiempirical theory in conjunction with the well known incremental load concepts.

APPLICATION OF SEMIEMPIRICAL THEORIES TO SOME EXISTING DATA

The experimental data in figure 2 are those reported in reference 19 for the ply transverse modulus $E_{\ell 22}$. The dashed line in this figure was obtained by applying the finite element method to a square array of filaments (ref. 19). The solid line is the result predicted by the semiempirical theory with values for the correlation coefficients β_f and β_m as noted in the figure. The agreement between semiempirical theory and the experimental data is quite good for a large range of k_f values. If the residual stress and bond strength vary appreciably over some range of k_f values, then different values of the correlation coefficients might be needed in different portions of this range.

The experimental data in figure 3 are those reported in reference 19 for ply transverse failure stress $S_{\ell 22T}$. The dashed line in this figure was obtained using the finite element method and a square array assuming complete interfacial bond (ref. 19). The
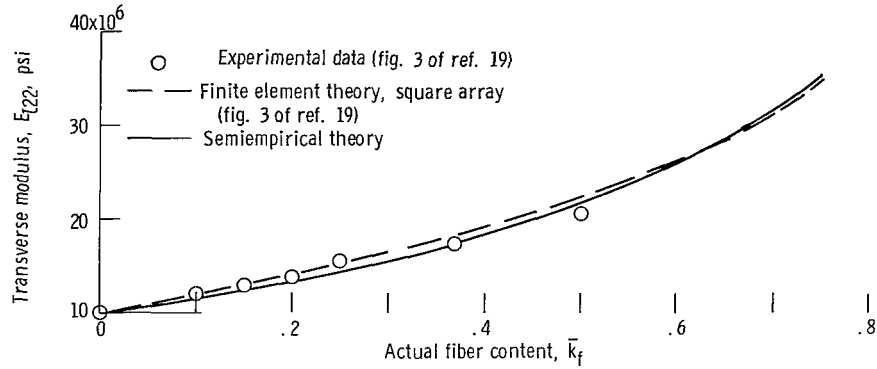
Figure 2. - Comparisons for transverse modulus of boron-aluminum unidirectional fiber composites. Filament modulus, $E_f = 55\times10^6$ psi; matrix modulus, $E_m = 10\times10^6$ psi; filament correlation coefficient, $\beta_f = 1.0$; matrix correlation coefficient, $\beta_m = (1.0/k_m)^{1/6}$; void volume ratio, $k_v = 0$.
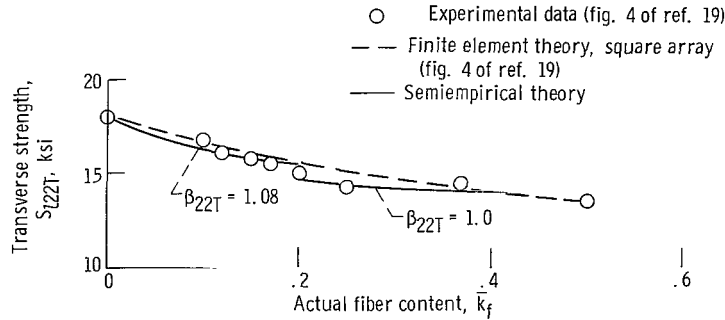

Figure 3. - Comparisons for transverse strength of boron-aluminum unidirectional fiber composites. Matrix tensile strength, $S_{mT} = 18\,000$ psi (ref. 19); filament modulus, $E_f = 55\times10^6$ psi (ref. 19); matrix modulus, $E_m = 10\times10^6$ psi (ref. 19); filament correlation coefficient, $\beta_f = 1.0$; matrix correlation coefficient, $\beta_m = (1.0/k_m)^{1/6}$; void volume ratio, $k_v = 0$.

solid lines are those predicted by the semiempirical theory with correlation coefficient β_{22T} (eq. (B9)) values as noted in the figure. Two values are required for β_{22T} in this case: $\beta_{22T} = 1.08$ for the range $0 \leq k_f \lesssim 0.2$ and $\beta_{22T} = 1.0$ for $0.2 \leq k_f \lesssim 0.5$. Distinct values of the correlation coefficient in a certain k_f range are more typical; this is also one of the basic hypotheses for using semiempirical theories.

It might appear, at first glance from the results in figure 3, that the finite element method is far superior to the semiempirical method in this case. However, the finite element method is far too complex and time consuming as compared with equation (B9). The complexity of the finite element method increases exponentially when it is called on to handle an anisotropic in situ matrix, anisotropic fibers, and void effects.

The experimental data in figure 4 are the room temperature data reported in reference 20 for ply longitudinal tensile stress $S_{\ell 11T}$. The values of the correlation coef-
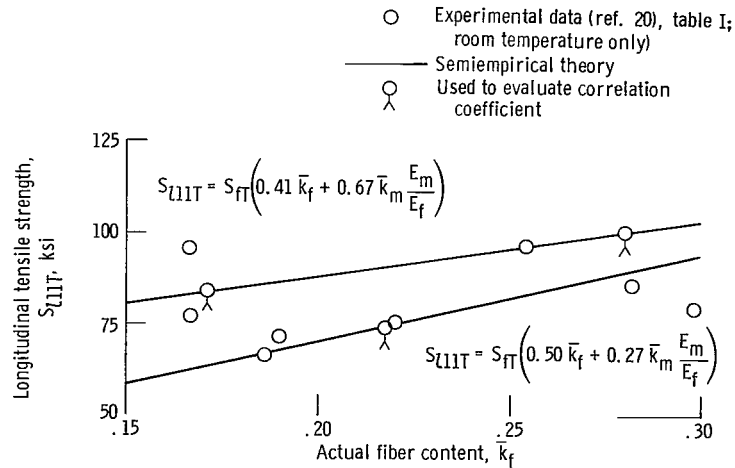
8

Figure 4. - Comparisons for longitudinal tensile strength of boron-aluminum unidirectional fiber composites. Filament tensile strength, S_{fT} = 510 ksi; filament modulus, E_f = 59x10^6 psi; matrix modulus, E_m = 10x10^6 psi; void volume ratio, k_v = 0.

ficients β_{fT} and β_{mT} entering equation (B7) and the experimental points selected to evaluate the correlation coefficients are noted in the figure. Here, it is seen that values of the correlation coefficients can be selected for good theory-experiment agreement through any desired points.

THERMOELASTIC PROPERTIES OF BORON-ALUMINUM UFC

The constituent properties employed to generate ply thermoelastic properties for composite characterization and design are given in table I. The experimental data used to select the correlation coefficients are shown in table II. The corresponding values of the correlation coefficients entering the various equations in appendix A are listed in table III.

Thermal Properties

Ply thermal properties (three conductivities, three coefficients of thermal expansion, and the heat capacity) as functions of fiber content and assuming zero voids are presented in figure 5. The results in this figure were obtained using the appropriate equations in appendix A in conjunction with the constituent properties of table I and the correlation coefficient values of table III. As can be seen in figure 5, the heat capacity increases as the fiber content increases. The remaining thermal properties decrease

9

TABLE I. - MEASURED VALUES OF

CONSTITUENT PROPERTIES

Properties	Boron fiber	6066-T6 aluminum matrix
E, 10^6 psi	60.0	10
ν, ratio	0.2	0.3
α, 10^{-6} in./in./°F	2.8	12.9
K, Btu/hr-ft^2-°F/in.	22.3	84
H, Btu/lb/°F	0.31	0.23
ρ, lb/in.^{3}	0.085	0.98
S, ksi	460	[a]52
ϵ_{mpC}, in./in.	-----	[a]0.0052
ϵ_{mpS}, in./in.	-----	[a]0.00905

[a]Values at yield.

TABLE II. - MEASURED VALUES

OF COMPOSITE PROPERTIES

(REF. 22)

[Fiber volume ratio, 0.5.]

Property	Value, psi
$E_{l\,11}$	34.2×10^6
$E_{l\,22}$	23.4×10^6
$S_{l\,11T}$	164×10^3
$S_{l\,11C}$	183
$S_{l\,22T}$	13.9
$S_{l\,22C}$	15.3
$S_{l\,12S}$	15.6

TABLE III. - SOME BASIC PARAMETERS

AND CORRELATION COEFFICIENTS FOR

THERMOELASTIC PROPERTIES

Property	Value
Basic parameters	
N_f	1
d_f	0.004
k_v	0
k_f	$0.35 < k_f < 0.75$
Correlation coefficients	
β_f	1.0
β_m	4.0
β'_f	[a]1.0
β'_m	[a]2.0
β''_f	[a]1.0
β''_m	[a]2.0
$\tilde{\beta}_f$	[a]1.0
$\tilde{\beta}_m$	[a]2.0
β_{kv}	[a]1.0
β_{k1}	[a]1.0
β_{k2}	[a]1.0
β_{k3}	[a]1.0

[a]Estimate.

Figure 5. - Boron-aluminum unidirectional thermal properties. Void volume ratio, $k_v = 0$.

with increasing fiber content. The literature is virtually void of measured data of thermal properties of fiber-reinforced metals.

Elastic Properties

Ply elastic properties (normal moduli, shear moduli, and Poisson ratios) are plotted in figure 6 as functions of fiber volume ratio and assuming zero void content.
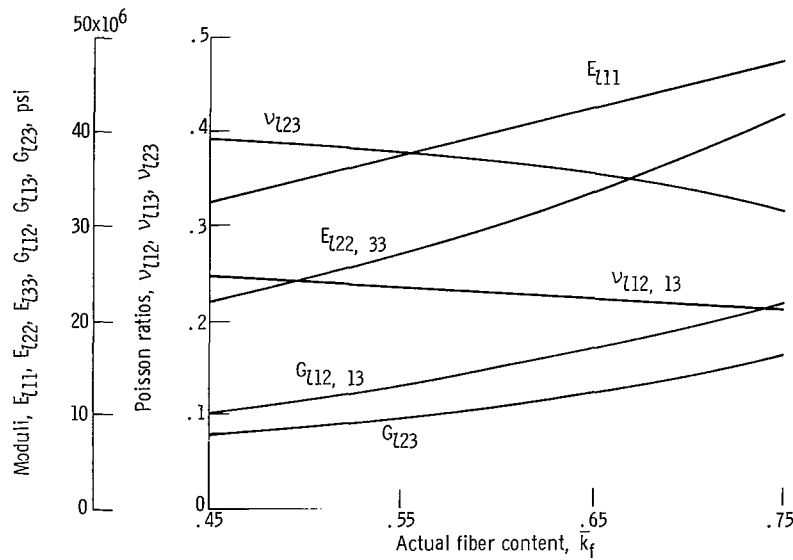
Figure 6. – Boron-aluminum unidirectional elastic properties. Void volume ratio, $k_v = 0$.

The results in this figure were obtained from the appropriate equations in appendix A using the constituent properties given in table I, the measured composite properties presented in table II, and the correlation coefficients of table III. It can be seen in figure 6 that the moduli are increasing functions of fiber content while the Poisson ratios are decreasing functions. Note, particularly, that the transverse moduli $E_{\ell 22, 33}$ increase rapidly with increasing fiber content.

An extensive amount of experimental data is available for the longitudinal modulus $E_{\ell 11}$, and these data are in agreement with rule of mixtures predictions. Measured data for the remaining elastic constants are meager and more organized measured data are needed.

12

PLY STRENGTHS

Ply strength, in the sense used here, denotes that stress level in the ply which causes incipient material nonlinear response (ref. 18).

The ply strengths are characterized by the ply uniaxial strengths and a combined stress strength criterion (ref. 18). The constituent materials, the properties given in table I, the measured data in table II, and the correlation coefficients in table IV were used in conjunction with the equations in appendix B to generate ply strengths.

TABLE IV. - CORRELATION COEFFICIENTS

FOR STRENGTH PROPERTIES

[Application limit, $0.35 < k_f < 0.75.$]

Correlation coefficient	Value	Correlation coefficient	Value
β_{fT}	0.58	a_1	8.33
β_{fC}	1.00	a_2	52 000
β_{mT}	1.00	$K'_{l\,12TT}$	[a]1.0
β_{mC}	1.00	$K'_{l\,12CT}$	[a]1.0
β_{22T}	0.313	$K'_{l\,12TC}$	[a]1.0
β_{22C}	0.343	$K'_{l\,12CC}$	[a]1.0
β_{12S}	0.462		

[a]Estimate.

Uniaxial Strengths

Five ply strengths $(S_{l\,11T},\ S_{l\,11C},\ S_{l\,22T},\ S_{l\,22C},$ and $S_{l\,12S})$ are required to characterize the uniaxial strength behavior of a ply (fig. 1). The graphs of these strengths as functions of fiber content when assuming zero voids are shown in figure 7. Measured values from table II are also shown in this figure. The curve labeled $S_{l\,11D}$ in figure 7 limits the longitudinal compressive stress according to the debonding model (ref. 18). The results in figure 7 show that the $S_{l\,11C}$ is matrix controlled for $k_f < 0.5$ and that it is debonding controlled for $k_f > 0.5$; $S_{l\,22T},\ S_{l\,22C},$ and $S_{l\,12S}$ are relatively insensitive to fiber content in the range investigated. This is in contrast to the behavior of these same limit stresses which are quite sensitive to fiber content for nonmetallic matrix composites.

Ply strengths for a ply with 5 percent void volume content are plotted in figure 8 using the correlation coefficients from table IV since the theory accounts directly for
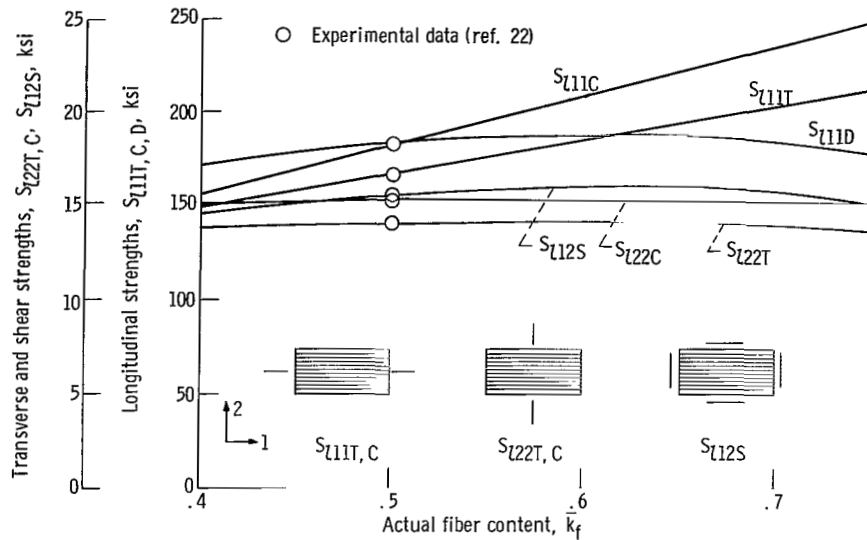
Figure 7. - Boron-aluminum uniaxial strengths. Void volume ratio, $k_v = 0$.
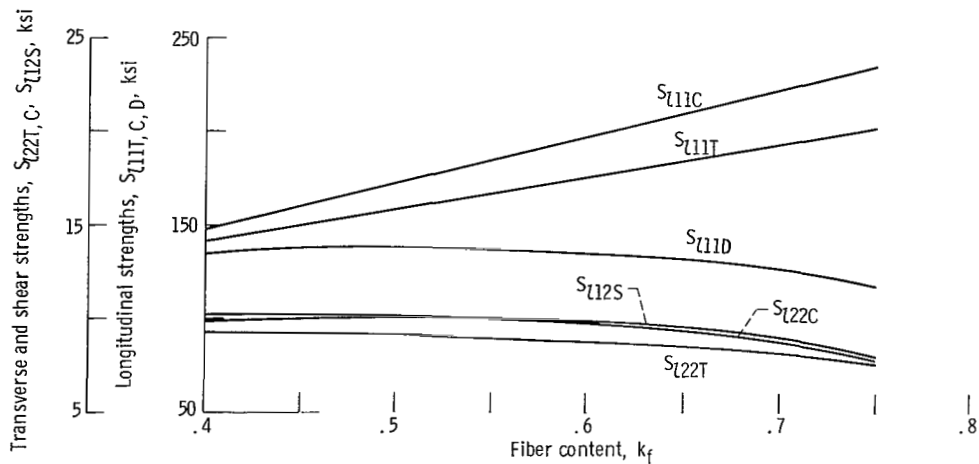
Figure 8. - Boron-aluminum uniaxial failure strengths. Void volume ratio, $k_v = 0.5$.

the void effects. The results in figure 8 show that $S_{\ell 11D}$, $S_{\ell 22T}$, $S_{\ell 22C}$, and $S_{\ell 12S}$ are slightly sensitive to fiber content at high fiber packing densities. The results also show that the ply longitudinal compressive strength is limited by debonding in plies with 5 percent void content.

Comparing similar curves in figures 7 and 8, it is readily seen that the presence of voids (porosity) has deleterious effects on ply strengths - particulary $S_{\ell 11D}$, $S_{\ell 22T}$, $S_{\ell 22C}$, and $S_{\ell 12S}$.

Researchers in the field of fiber-reinforced metals have investigated extensively the uniaxial longitudinal tensile strength for various fiber metallic matrix systems. However, measured values of the other uniaxial strength properties are either rare or non-

14

existent. Measured data for the uniaxial strengths $S_{\ell11C}$, $S_{\ell22T}$, $S_{\ell22C}$, and $S_{\ell12S}$ are mandatory if fiber-reinforced metals are to become serious contenders for structural components and if their interfacial characteristics are to be better understood.

Ply Combined-Stress Strength Criterion

The combined-stress strength criterion for the ply used herein is described in equation (B12). The coupling coefficient $K_{\ell12}$ is defined by equation (B13) and values for the correlation coefficients $K'_{\ell12\alpha\beta}$ (α, β = T, C) are given in table IV.
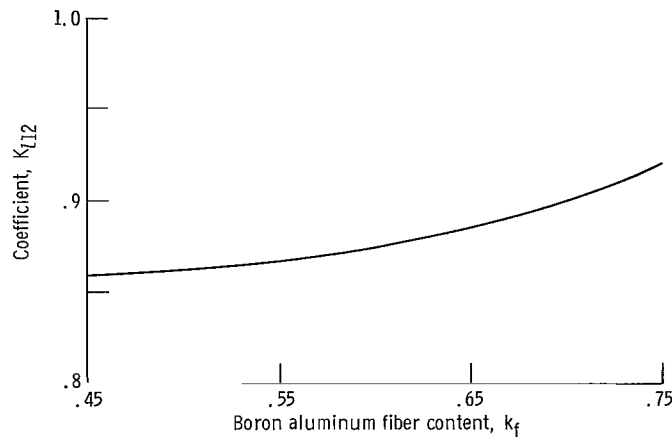
Figure 9. – Boron aluminum combined-stress strength coefficient (applicable for $0 \leq k_v < 0.20$).

A plot of the coupling coefficient $K_{\ell12}$ as a function of fiber volume ratio is given in figure 9. This coefficient is relatively insensitive to void content. The ply combined-stress strength criterion for a ply of 50 percent fiber volume content and zero voids is plotted in figure 10. Note that the $\sigma_{\ell22}$ stress scale is different from the $\sigma_{\ell11}$ scale in this figure. This causes the graph generated by the criterion to be distorted although it can be read more accurately this way. The various contours in the figure represent different levels of shear stress as noted. Measured values of the uniaxial ply strengths from table II are also shown in figure 10.

The results in figure 10 show that the ply combined-stress strength is not sensitive to small values of the ratio $\sigma_{\ell12}/S_{\ell12S}$. This means that in testing for uniaxial normal limit strengths, a small amount of shear stress has negligible effects on the results.

Failure envelopes for other fiber contents can be constructed by substituting corresponding ply uniaxial strengths from figure 7 and coupling coefficient values from fig-
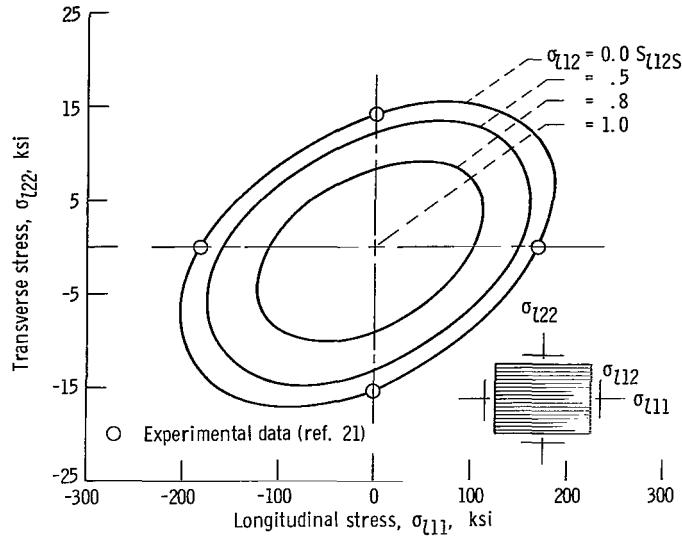
Figure 10. - Failure envelopes under combined-stress for boron-
aluminum. Fiber content, $k_f = 0.5$; void volume ratio, $k_v = 0$.

ure 9 in equation (B12). Figure 8 can be used, or an analogous one, for cases in which the plies contain voids.

There are no experimental data available for plies or unidirectional composites sub-
jected to combined stress. For this reason, the correlation coefficient $K'_{\ell\,12\alpha\beta}$ is as-
sumed to be one. Strategic experimental work in this area is needed for two important
reasons: (1) to verify the failure criterion of equation (B12) or to provide insight and
a basis for its modification, and (2) to generate measured data from which the correla-
tion coefficient $K'_{\ell\,12\alpha\beta}$ can be evaluated.

OFF-AXIS COMPOSITES

Off-axis composites are unidirectional composites whose fiber direction is offset
from the structural axis by a specified angle. The study of thermoelastic and strength
behavior of off-axis composites serves two purposes: (1) generation of design data and
(2) providing of additional insight into the composite structural behavior.

Plies or UFC Subjected to Off-Axis Loadings

Off-axis thermoelastic and strength characterization of a composite is readily de-
termined from its characterization along the ply's orthotropic axes using suitable
transformations such as equations (B16) to (B20) (see appendix B).

16

Off-Axis Ply Thermoelastic Properties

The strain-stress-thermal relations for an off-axis ply (assumed a thin plate) are given by

$$\left\{ \begin{array}{c} \epsilon_{cxx} \\ \epsilon_{cyy} \\ \epsilon_{cxy} \end{array} \right\} = \begin{bmatrix} \dfrac{1}{E_{cxx}} & -\dfrac{\nu_{cyx}}{E_{cyy}} & -\dfrac{\nu_{csx}}{G_{cxy}} \\ -\dfrac{\nu_{cxy}}{E_{cxx}} & \dfrac{1}{E_{cyy}} & -\dfrac{\nu_{csy}}{G_{cxy}} \\ -\dfrac{\nu_{cxs}}{E_{cxx}} & -\dfrac{\nu_{cys}}{E_{cyy}} & \dfrac{1}{G_{cxy}} \end{bmatrix} \left\{ \begin{array}{c} \sigma_{cxx} \\ \sigma_{cyy} \\ \sigma_{cxy} \end{array} \right\} + \Delta T \left\{ \begin{array}{c} \alpha_{cxx} \\ \alpha_{cyy} \\ \alpha_{cxy} \end{array} \right\}$$

or

$$\{\epsilon_{cx}\} = [E_{cx}]\{\sigma_{cx}\} + \Delta T \{\alpha_{cx}\} \tag{3}$$

where ϵ, σ, and ΔT are the strain, stress, and the temperature above some reference value; and E, G, ν, and α are the normal modulus, shear modulus, Poisson ratio, and thermal coefficient of expansion, respectively. Note the Poisson ratios ν_{csx} and ν_{csy}. These ratios couple in-plane normal and shear responses. Note also the thermal coefficient of expansion α_{cxy}. Coefficients such as ν_{csx}, etc., and α_{cxy} are present only in materials exhibiting anisotropic behavior. In equation (3), the following relations hold:

$$\frac{\nu_{cyx}}{E_{cyy}} = \frac{\nu_{cxy}}{E_{cxx}}; \qquad \frac{\nu_{cxs}}{E_{cxx}} = \frac{\nu_{csx}}{G_{cxy}}; \qquad \frac{\nu_{cys}}{E_{cyy}} = \frac{\nu_{csy}}{G_{cxy}} \tag{4}$$

The matrices $[E_{cx}]$ and $\{\alpha_{cx}\}$ in equation (3) are derived from the transformation equations (B16) to (B20). Plots for the coefficients α_{cxx}, α_{cyy}, and α_{cxy}, as functions of the angle and for a particular fiber content ($\bar{k}_f = 0.5$, $k_v = 0$), are shown in figure 11. Analogous plots for the coefficients E, G, and ν are shown in figure 12. The geometry of the off-axis ply and the ranges of the angle are also shown in these figures. The points to be noted in figures 11 and 12 are as follows:

(1) The anisotropic coefficients α_{cxy}, ν_{csx}, and ν_{csy} vanish when the ply material axes (axes 1-2) coincide with the ply structural axes (axes x-y).
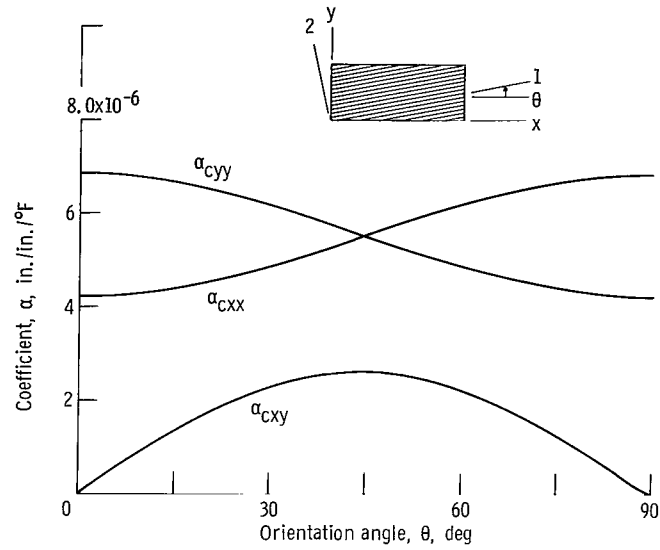
17

Figure 11. - Thermal coefficients of expansion for off-axis uni-directional boron aluminum composites. Actual fiber content, $\bar{k}_f = 0.5$; void volume ratio, $k_v = 0$.
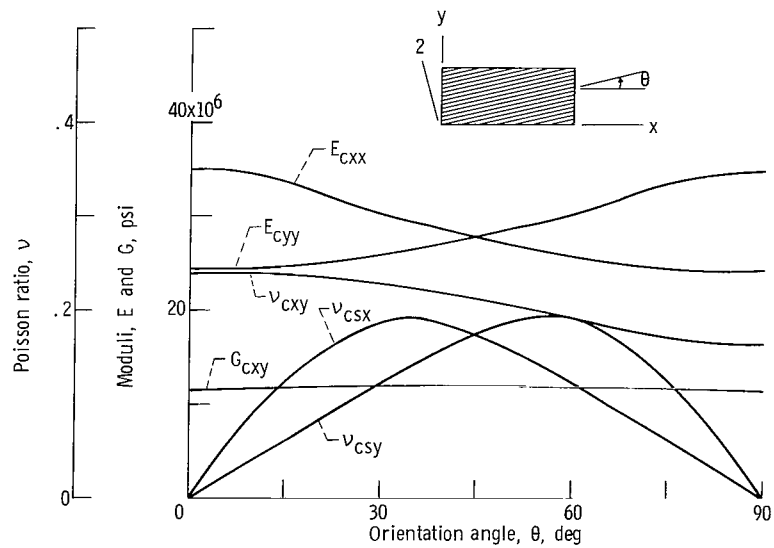
Figure 12. - Moduli and Poisson ratios for off-axis unidirectional boron-aluminum composites. Actual fiber content, $\bar{k}_f = 0.5$; void volume ratio, $k_v = 0$.

18

(2) The anisotropic coefficients except the shear modulus attain significant magnitudes at a certain angle.

At these angles, residual stresses and severe end effects can be induced. Residual stresses and end effects are the primary obstacles in theory-experiment correlation and in interpreting experimental data.

Plots for other fiber contents can be obtained by using figures 5 and 6 in conjunction with equations (B16) to (B20). In the case of voids, plots analogous to those of figures 5 and 6 need to be generated first from the equations in appendix A for the specific void content. Heat conductivities for off-axis plies can also be obtained by transformation. The ply heat capacity remains invariant.

Again, strategic experimental data to check the transformation equations are needed.

Off-Axis Ply Failure Envelopes

Plies or UFC subjected to off-axis loadings possess four distinct failure envelopes - namely, normal tensile load, normal compressive load, positive shear load (tends to extend the fibers), and negative shear load (tends to compress the fiber) (ref. 18). These envelopes are generated using values from figures 7 and 9 and table IV in equation (B14) for normal loadings and equation (B15) for shear loadings.

Plots of equation (B14) as a function of the angle and for a specific fiber volume content ($\bar{k}_f = 0.5$, $k_v = 0$) are presented in figure 13. The filament and loading direc-
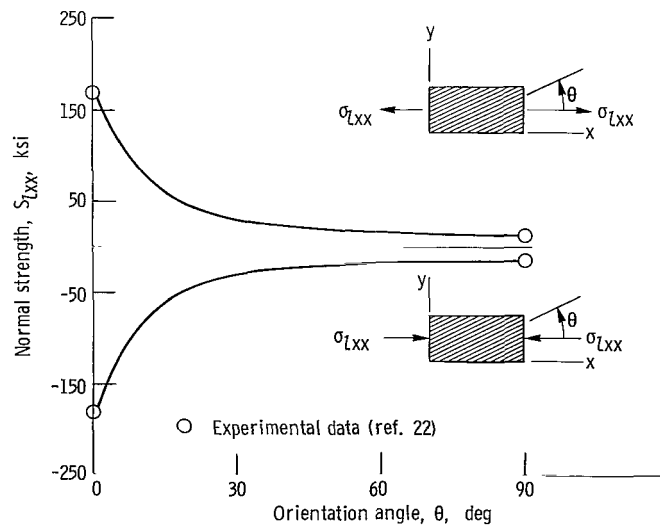
Figure 13. - Boron-aluminum off-axis normal load failure envelopes. Actual fiber content, $\bar{k}_f = 0.5$; void volume ratio, $k_v = 0$.

tions and the experimental strength points ($\theta = 0°$ and $90°$) from table II are also shown in the figure. The results in figure 13 indicate a rapid drop in the ply strength as load direction deviates from the filament direction for both normal tensile and compressive loads. This clearly illustrates the importance of fiber alinement when testing or designing for longitudinal strength.

Analogous plots for shear load (eq. (B15)) are presented in figure 14. The filament and loading directions and the experimental strength points from table II are shown in the figure. The upper portion of the figure is for positive shear load (as noted) while
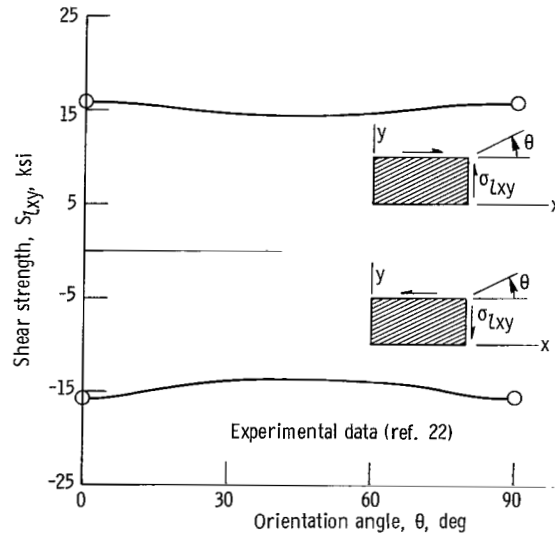
Figure 14. – Boron–aluminum off-axis shear load failure envelopes. Actual fiber content, $\bar{k}_f = 0.5$; void volume ratio, $k_v = 0$.

the lower part is for negative load. The results in figure 14 indicate that the failure envelopes for off-axis plies are insensitive to shear loads. Experimental verification of the last comment is still needed.

A last comment to be made for ply off-axis failure envelopes is that for each point on the uniaxial strength curves in figures 13 and 14 there corresponds a unique point in figure 10. For actual design purposes the ply off-axis failure envelopes are redundant and rarely used. However, these envelopes provide an insight into composite strength behavior. This will become clear from the discussion in the next section.

Effects of Intralaminar Shear and Transverse Strengths on

Ply Off-Axis Failure Envelopes

The ply off-axis failure envelopes can be utilized to yield additional useful information about composite strength behavior. This is illustrated in figure 15 where the ply off-axis failure strength for normal load and $\bar{k}_f = 0.5$ is plotted as a function of the angle for various combinations of the intralaminar shear and transverse uniaxial strengths. The standard curve in figure 15 is the curve labeled 1. The corresponding measured values from table II are shown in the figure at $\theta = 0^\circ$ and 90°. The curves corresponding to intralaminar shear variations are labeled 2, 3, 4, and 5. The curves corresponding to transverse strength variations are labeled 6, 7, and 8.

Three important observations can be made using figure 15:

(1) The effect of fiber misalinement can be minimized with large increases in ply intralaminar shear strength. This finding is encouraging with respect to short fiber and whisker reinforced composites.

Experimental data (ref. 22)

Curve	S_{l22T}, ksi	S_{l12S}, ksi
1	14	15.6
2	14	20.0
3	14	30.0
4	14	40.6
5	14	60.0
6	20	15.6
7	40	15.6
8	60	15.6

Figure 15. - Off-axis normal load failure envelopes for various values of S_{l22T} and S_{l12S} of boron-aluminum composites. Actual fiber content, $\bar{k}_f = 0.5$; void volume ratio, $k_v = 0$.
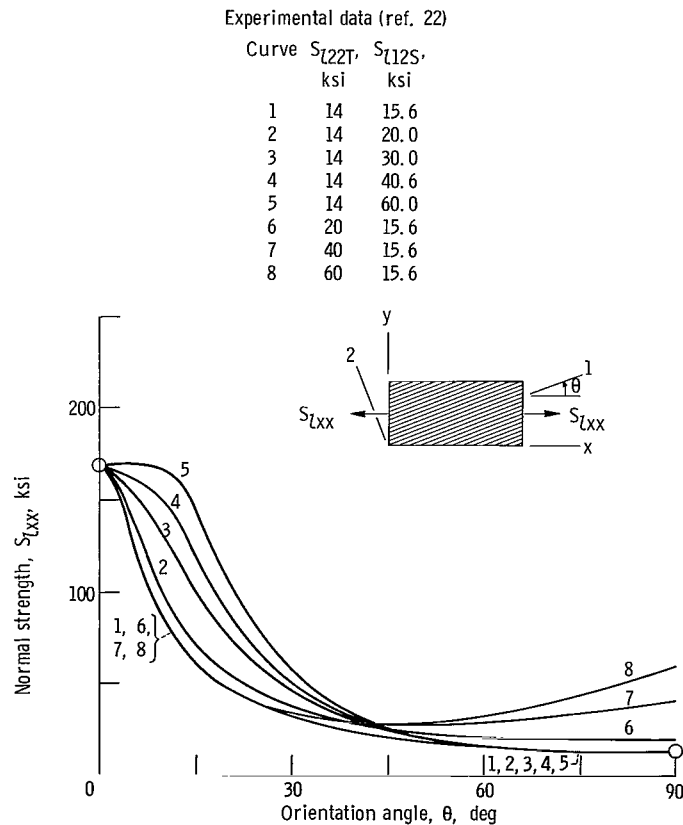
(2) The ply off-axis failure envelope is sensitive to transverse strength in the $30^O < \theta \lesssim 90^O$ range.

(3) The ply in angle-ply composites has four predominant failure modes: these are longitudinal tension or compression, $0^O \leq \theta < 3^O$; intralaminar shear, $3^O \lesssim \theta \lesssim 30^O$; shear or transverse tension or compression, $30^O < \theta < 60^O$; transverse tension or compression, $60^O \lesssim \theta < 90^O$. These observations stem from the fact that a ply within an angle-ply composite is reinforced by its adjacent plies, relative to intralaminar shear and transverse failure stress modes. This type of reinforcement has the same effects on the ply off-axis failure envelope as do the variations of intralaminar shear and transverse strengths noted in figure 15.

Appropriate experimental data are lacking for ply failure envelopes for fiber-reinforced metals of potential use for structural components. Also, experimental data to verify the three points previously mentioned are needed.

SOME PROPERTIES OF ANGLE-PLY COMPOSITES

Properties of angle-ply composites are determined theoretically by laminate theories (refs. 24 to 26). In general, lamination theory yields the strain-stress thermal relations, axial stiffnesses, coupling stiffnesses, bending stiffnesses, and thermal forces. Herein, only results for the thermal coefficients of expansion and the elastic constants of a symmetric (in-plane shear and bending) angle-ply composite are presented. The results are for a composite with 50 percent fiber content, zero void content, and the stacking sequence $(\theta, -\theta, -\theta, \theta)$. The results were obtained using the constituent properties in table I and equations (B21) and (B22).

Plots of the thermal coefficients of expansion α_{cxx} and α_{cyy} as a function of the ply angle are shown in figure 16. Analogous plots for the elastic constants are shown
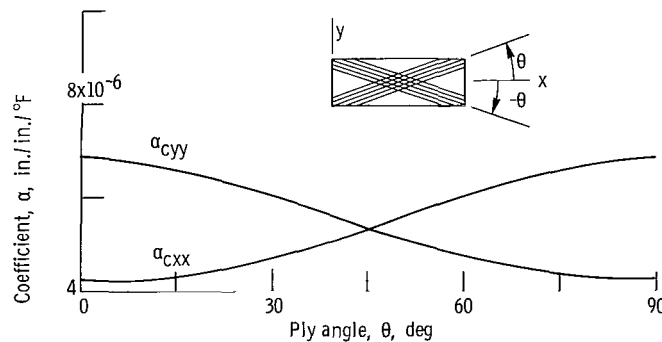

Figure 16. - Thermal coefficients of expansion for boron-aluminum angle-ply composites. Actual fiber content, $\bar{k}_f$ = 0.5; void volume ratio, k_v = 0.
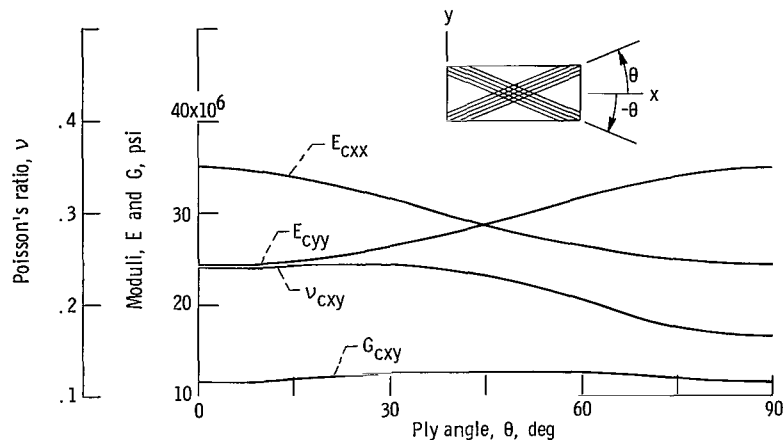
Figure 17. – Elastic constants for boron-aluminum angle-ply composites. Actual fiber content, $\bar{k}_f = 0.5$; void volume ratio, $k_v = 0$.

in figure 17. Angle-ply composites with symmetric stacking sequence relative to in-plane shear do not have coefficients such as α_{cxy} and ν_{csx}, etc. The results in figure 17 indicate that the shear modulus of symmetric angle-ply composites, with low (E_{cxx}/E_{cyy}) ratio, is relatively insensitive to ply orientation angle.

Particular care should be taken in fabricating angle-ply composites. Factors such as ply stacking sequence, slight fiber misalinements in the ply, slight ply misorientation from the structural axes, and variation in fiber and void content from ply to ply result in several distinct coupling responses of the type described in reference 27. Here, suffice it to say, that all these coupling responses affect the structural response of angle-ply composites. This makes it difficult (if not impossible) to interpret experimental results and to correlate theories with experimental data.

Experimental data for angle-ply fiber-reinforced metallic-composites is limited. Strategic experiments to obtain some measure of the various coupling response effects on composite structural behavior will prove very beneficial.

ADDITIONAL ASPECTS OF COMPOSITE CHARACTERIZATION MECHANICS

Several other aspects of composite characterization mechanics, which have not been dealt with specifically herein, merit mentioning. Some others need verification, modification, or extension, and then there are those yet to be developed. Some of these are mechanics for constituent load transfer at the interface, composite toughness, composite internal damping, lamination edge and internal residual stresses, geometry and material nonlinearities (including plastic behavior), temperature and time effects in-

cluding creep, and cyclic loading and fatigue. References 28 to 37 should provide some direction in all these areas.

A deeper assessment and carefully formulated programs (both analytical and experimental) to investigate various aspects of the previously mentioned areas will be of great service to the fiber-reinforced metals research and design community.

OTHER DESIGN FACTORS

Composite thickness, interfiber spacing, composite density, delamination, and buckling parameters are important variables in component design. Some of these variables can be related to fiber geometry, packing array, void content, and other constituent properties by elementary relations described in reference 21. Results are presented here for a boron aluminum composite.

The ply thickness is plotted in figure 18 as a function of the actual fiber content and
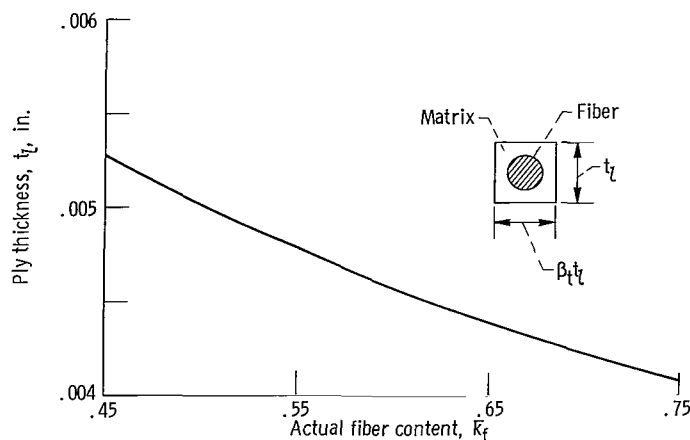
Figure 18. - Boron-aluminum ply thickness. Packing array parameter, $\beta_t = 1.0$; void volume ratio, $k_v = 0$.

for a square array. The curve in this figure was generated from equation (A4) with $N_f = 1$, $\beta_t = 1$ (the parameter β_t can be selected from measured data for different arrays; ref. 20, and $d_f = 0.004$ inch. Analogous plots for boron fibers with different diameters can readily be generated from equation (A4) The curve in figure 18 indicates that the ply thickness decreases rapidly with increasing fiber content. This is significant because the buckling resistance of a structural component varies with the thickness cubed. Note the presence of voids increases the ply thickness, if the apparent fiber volume remains constant.

A plot of the interfiber spacing against actual fiber content and for a square array

24
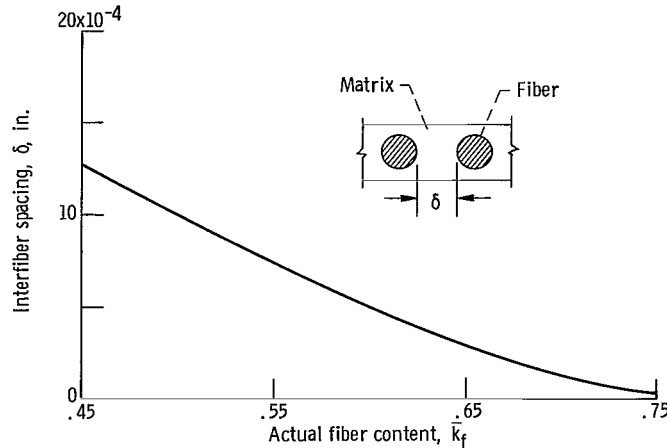
Figure 19. - Boron-aluminum interfiber spacing. Void volume ratio, $k_v = 0.$

is shown in figure 19. The curve in this figure was generated from equation (A3) with $d_f = 0.004$ inch. Analogous plots with different fiber diameters can be readily generated from equation (A3). The results in figure 19 show a rapid decrease in the interfiber spacing particularly at high packing densities. The designer of fiber composites should keep the curve in figure 19 in mind. This curve is important because transverse strength, intralaminar shear strength, and fiber-matrix load transfer depend strongly on the interfiber spacing.

The composite weight density ρ_c is plotted against actual fiber content $\bar{k}_f$ in figure 20. As can be seen in the figure the composite density is a linearly decreasing function of the actual fiber content for the boron-aluminum composite. The presence of voids in a composite reduces its weight density if the actual fiber content is held constant.
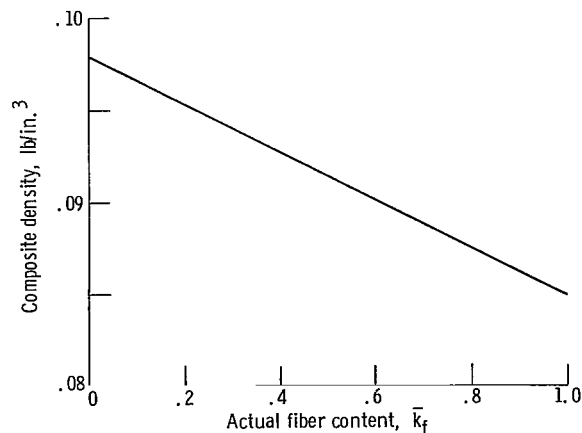
Figure 20. - Boron-aluminum composite density. Void volume ratio, $k_v = 0.$

25
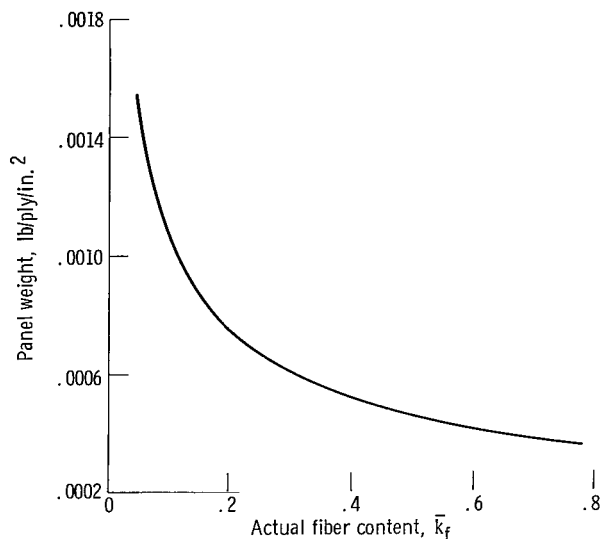
Figure 21. - Boron-aluminum ply weight. Void volume ratio, $k_v = 0$.
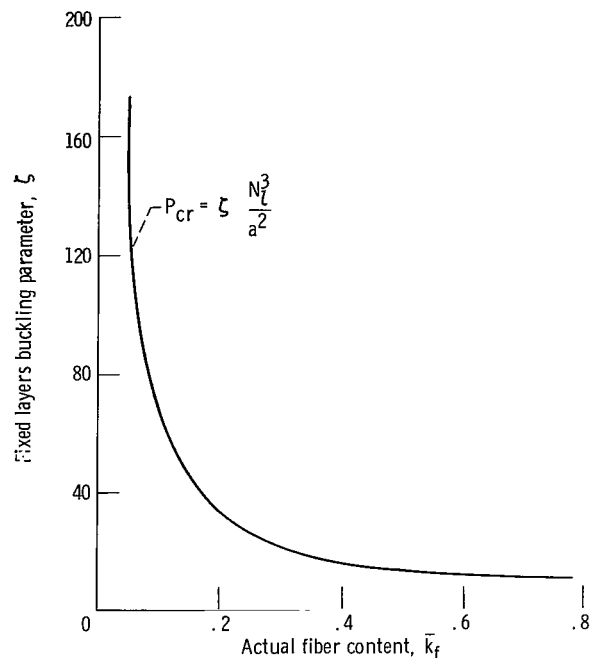
Figure 22. - Boron-aluminum buckling parameter for simply supported square plates. Void volume ratio, $k_v = 0$.

An interesting parameter in trade-off and efficiency studies is the ply weight per unit area. This parameter is plotted against $\bar{k}_f$ in figure 21 for square array packing. The resulting curve for this case shows that the ply weight decreases approximately in a hyperbolic fashion with increasing $\bar{k}_f$.

The buckling resistance of a structural component is another parameter commonly employed in trade-off and efficiency studies. The bucling parameter ζ for a square simply supported plate is plotted against $\bar{k}_f$ in figure 22. The plate in this case is loaded along the fiber direction and is made from unidirectional material with square array packing and a fixed number of layers (ref. 21). The plot in this figure shows a very rapid decrease of the buckling load at low fiber contents and a mild decrease at $\bar{k}_f > 0.3$ with increasing fiber content. The decrease of the buckling parameter at the low fiber volume contents comes from the fact that buckling resistance varies with the thickness cubed while it varies linearly with modulus. As is illustrated in figure 18, the thickness decreases as the fiber content increases for the square array fiber packing. The important point to be kept in mind from this discussion is that low fiber content composites are more efficient in resisting buckling when the number of layers is the limiting condition. Analogous results when the weight is held constant are plotted in figure 23. The curve in this figure shows that the buckling load is approximately a parabolic increasing function of $\bar{k}_f$ and does not possess an optimum. The conclusion

26

Figure 23. – Boron-aluminum weight buckling parameter for simply supported square plate. Void volume ratio, $k_v = 0$.

Figure 24. – Boron-aluminum transverse shear delamination parameter. Void volume ratio, $k_v = 0$.

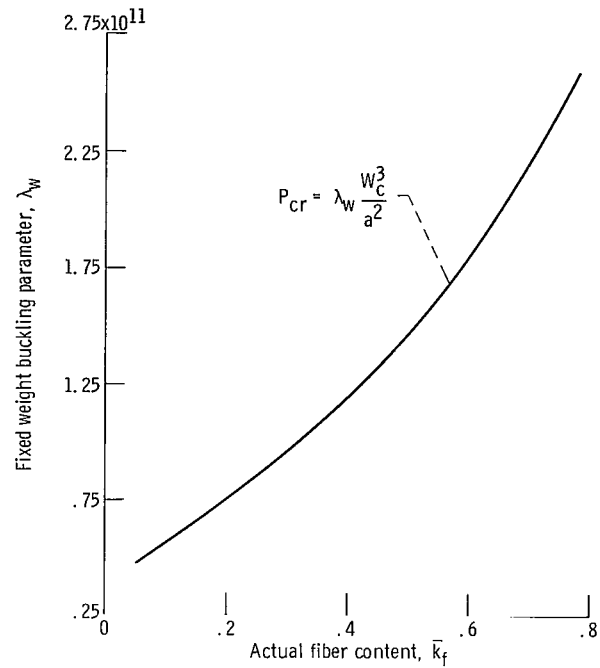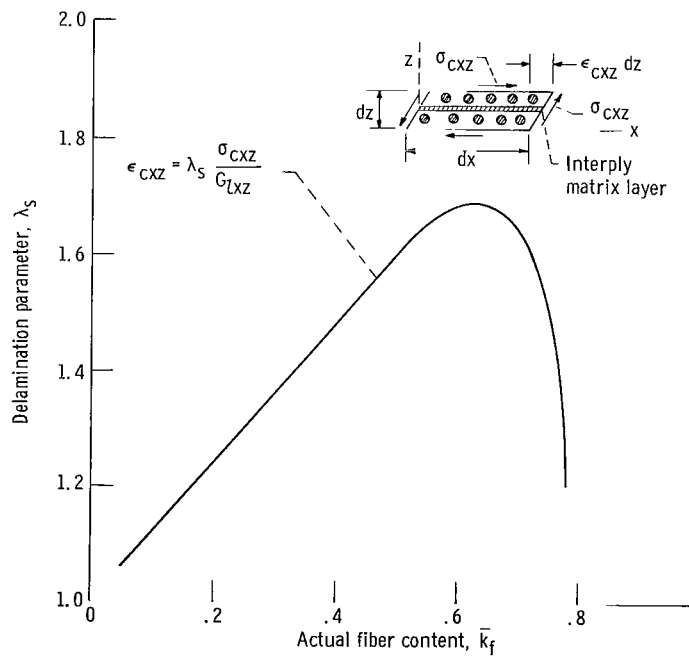in this case is that high fiber content composites resist buckling loads more efficiently when the composite weight is the limiting condition.

Ply delamination, either due to adjacent ply relative rotation (scissoring effect) or interply transverse shear (through the thickness, horizontal), is a possible failure mode for multilayered composites (ref. 21). The delamination parameter for transverse shear is plotted against $\bar{k}_f$ in figure 24. The equation of the curve and the corresponding geometry are also shown in the figure. The notation in the equation is as follows: ϵ_{cxz}, interply transverse shear strain; λ_s, delamination parameter; σ_{cxz}, interply transverse shear stress; $G_{\ell xz}$, interply shear modulus in the x-z plane (ref. 21). Replace x with y for the equation in the y-z plane. The resulting curve in figure 24 indicates that the delamination parameter for transverse shear is very sensitive to $\bar{k}_f$ with a maximum $\bar{k}_f \simeq 0.65$. This means that low and very high fiber content boron-aluminum composites are less susceptible to delamination than are those of intermediate $\bar{k}_f$ values. Results for the delamination parameter due to adjacent ply relative rotation are not presented because evaluation of this parameter requires specific measured data which are not available at this time. Reference 21 describes the type of data needed. Measured data for several of these factors and theory-experiment correlation are still needed.

CONCLUDING REMARKS

The semiempirical theories developed primarily for nonmetallic composites can also be employed in characterization and design mechanics for metallic composites which exhibit linear or approximately linear behavior. This is important in optimum designs of components made from these materials where the fiber content is taken as a design variable. It is also important in designing experiments and interpreting experimental results.

The results of this investigation lead to the following conclusions concerning boron fiber - aluminum matrix composites:

1. The uniaxial strengths $S_{\ell 11D}$, $S_{\ell 22T}$, $S_{\ell 22C}$, and $S_{\ell 12S}$ are relatively insensitive to fiber content in the range investigated when voids are absent but are sensitive at high fiber contents in the presence of voids.

2. The longitudinal compressive strength is limited by both matrix yield ($\bar{k}_f < 0.5$) and debonding ($\bar{k}_f > 0.5$) in the absence of voids. This strength is governed by debonding ($0.40 < \bar{k}_f < 0.75$) when the void content is about 5 percent.

3. The failure envelopes for off-axis normal loadings show rapid loss of strength when the angle between fiber and load directions increases in the $1^o < \theta < 30^o$ range. The strength remains practically invariant at angles greater than 30°.

4. The failure envelopes for off-axis shear loadings are practically invariant with angle.

5. The normal tensile load failure envelope is quite sensitive to variations in intralaminar shear strength for load angles less than 30° and to variations in transverse tensile strength for load angles greater than 45°.

6. The predominant failure modes for off-axis normally loaded composites are longitudinal tension or compression when $0^\circ \leq \theta < 3^\circ$, intralaminar shear when $3^\circ \lesssim \theta < 30^\circ$, intralaminar shear or transverse tension or compression when $30^\circ \lesssim \theta \lesssim 60^\circ$, and transverse tension or compression when $60^\circ < \theta \leq 90^\circ$.

7. The shear modulus of off-axis and angle-ply composites is practically invariant with angle at low E_{l11}/E_{l22} ratios.

8. The ply thickness, interfiber spacing, composite density, and ply weight per unit area decrease with increasing fiber content.

9. The buckling load of a simply supported square plate made from a unidirectional boron aluminum composite, in which fibers are arranged in a square array and which is loaded in the plane of the plate, decreases with increasing fiber content when the number of plies is held constant but increases when the weight is held constant.

10. The delamination criterion indicates that the transverse shear strain in the matrix increases with fiber content up to about 65 percent fiber content and then it decreases very rapidly.

11. Experimental data for thermal properties, transverse strength properties, and combined failure criteria are needed. Well defined programs to investigate temperature, time, material, and geometry nonlinearities, damping, impact, and cyclic loadings are required.

Lewis Research Center,
　　National Aeronautics and Space Administration,
　　　　Cleveland, Ohio, February 2, 1970,
　　　　　　129-03.

APPENDIX A

EQUATIONS FOR PLY GEOMETRIC, ELASTIC, AND THERMAL PROPERTIES

The equations of the semiempirical theory are given herein. Most of the detailed derivations are rather lengthy and are not included here; however, they are given in appendixes A and B of reference 26. It is assumed that the various thermoelastic properties of the constituents in their precomposite state are known. It is further assumed that the apparent filament volume ratio k_f is given. When the axiom that the volume (weight) of the whole equals the sum of its parts is used, it can be shown that

$$\overline{k}_f = (1 - k_v)k_f \tag{A1}$$

$$\overline{k}_m = (1 - k_f)(1 - k_v) \tag{A2}$$

where the barred quantities denote actual volume ratio. The interfiber spacing δ and the ply thickness t_l are, respectively, given by

$$\delta = \left[\left(\frac{\pi}{4\overline{k}_f} \right)^{1/2} - 1 \right] d_f \tag{A3}$$

and

$$t_l = \left(\frac{\pi N_f}{\overline{k}_f \beta_t} \right)^{1/2} \frac{d_f}{2} \tag{A4}$$

where β_t is the in situ array rectangle length to width ratio (ref. 21). Let the normal strain-stress - temperature relations along the orthotropic axes for ply, filament, and matrix be given, respectively, by

$$\{\epsilon_l\} = [E_l]\{\sigma_l\} + \Delta T\{\alpha_l\} \tag{A5}$$

$$\{\epsilon_f\} = [E_f]\{\sigma_f\} + \Delta T\{\alpha_f\} \tag{A6}$$

$$\{\epsilon_m\} = [E_m]\{\sigma_m\} + \Delta T\{\alpha_m\} \tag{A7}$$

The normal elastic properties and the thermal coefficients of expansion are given, respectively, by

$$[E_\ell] = [C_{f\ell}]^T[E_f][C_{f\ell}]\bar{k}_f + [C_{m\ell}]^T[E_m][C_{m\ell}]\bar{k}_m \tag{A8}$$

$$\{\alpha_\ell\} = [C_{f\ell}]^T\{\alpha_f\}\bar{k}_f + [C_{m\ell}]^T\{\alpha_m\}\bar{k}_m \tag{A9}$$

where

$$\{\sigma_\ell\} = \begin{Bmatrix} \sigma_{\ell 11} \\ \sigma_{\ell 22} \\ \sigma_{\ell 23} \end{Bmatrix}; \quad \{\epsilon_\ell\} = \begin{Bmatrix} \epsilon_{\ell 11} \\ \epsilon_{\ell 22} \\ \epsilon_{\ell 33} \end{Bmatrix}; \quad \{\alpha_\ell\} = \begin{Bmatrix} \alpha_{\ell 11} \\ \alpha_{\ell 22} \\ \alpha_{\ell 33} \end{Bmatrix} \tag{A10}$$

$$[E_\ell] = \begin{bmatrix} \dfrac{1}{E_{\ell 11}} & -\dfrac{\nu_{\ell 21}}{E_{\ell 22}} & -\dfrac{\nu_{\ell 31}}{E_{\ell 33}} \\[2ex] -\dfrac{\nu_{\ell 12}}{E_{\ell 11}} & \dfrac{1}{E_{\ell 22}} & -\dfrac{\nu_{\ell 32}}{E_{\ell 33}} \\[2ex] -\dfrac{\nu_{\ell 13}}{E_{\ell 11}} & -\dfrac{\nu_{\ell 23}}{E_{\ell 22}} & \dfrac{1}{E_{\ell 33}} \end{bmatrix} \tag{A11}$$

Analogous equations for filament and matrix are obtained by replacing the subscripts in equations (A10) and (A11).

The filament and matrix stresses ply stress relations are

$$\begin{Bmatrix} \sigma_{f11} \\ \sigma_{f22} \\ \sigma_{f33} \end{Bmatrix} = \begin{bmatrix} \dfrac{1}{AE_{m11}\bar{k}_m} & \dfrac{1}{A}\left(\dfrac{\nu_{f21}}{C_f E_{f22}} - \dfrac{\nu_{m21}}{C_m E_{m22}}\right) & \dfrac{1}{A}\left(\dfrac{\nu_{f31}}{C_f E_{f33}} - \dfrac{\nu_{m31}}{C_m E_{m33}}\right) \\[2ex] 0 & \dfrac{1}{C_f} & 0 \\[2ex] 0 & 0 & \dfrac{1}{C_f} \end{bmatrix} \begin{Bmatrix} \sigma_{\ell 11} \\ \sigma_{\ell 22} \\ \sigma_{\ell 33} \end{Bmatrix}$$

$$\tag{A12}$$

31

$$
\left\{
\begin{array}{c}
\sigma_{m11} \\
\sigma_{m22} \\
\sigma_{m33}
\end{array}
\right\}
=
\left[
\begin{array}{ccc}
\dfrac{1}{BE_{f11}\overline{k}_f} & \dfrac{1}{B}\left(\dfrac{\nu_{m21}}{C_m E_{m22}} - \dfrac{\nu_{f21}}{C_f E_{f22}}\right) & \dfrac{1}{B}\left(\dfrac{\nu_{m31}}{C_m E_{m33}} - \dfrac{\nu_{f31}}{C_f E_{f33}}\right) \\[4mm]
0 & \dfrac{1}{C_m} & 0 \\[4mm]
0 & 0 & \dfrac{1}{C_m}
\end{array}
\right]
\left\{
\begin{array}{c}
\sigma_{l11} \\
\sigma_{l22} \\
\sigma_{l33}
\end{array}
\right\}
\tag{A13}
$$

where

$$
\left.
\begin{aligned}
A &= \left(\dfrac{1}{E_{f11}} + \dfrac{\overline{k}_m}{E_{m11}\overline{k}_f}\right) \\[3mm]
B &= \left(\dfrac{1}{E_{m11}} + \dfrac{\overline{k}_f}{E_{f11}\overline{k}_m}\right)
\end{aligned}
\right\}
\tag{A14}
$$

$$
\left.
\begin{aligned}
C_f &= \left(\dfrac{\overline{k}_f}{k_f}\right)\beta_f \\[3mm]
C_m &= \left(\dfrac{\overline{k}_m}{k_m}\right)\beta_m
\end{aligned}
\right\}
\tag{A15}
$$

The parameters β_f and β_m are chosen such that theory and experiment correlate as well as possible. When computing the ply thermal coefficients of expansion from equation (A9) use

$$
\left.
\begin{aligned}
C_f &= \left(\dfrac{\overline{k}_f}{k_f}\right)\widetilde{\beta}_f \\[3mm]
C_m &= \left(\dfrac{\overline{k}_m}{k_m}\right)\widetilde{\beta}_m
\end{aligned}
\right\}
\tag{A16}
$$

instead of equation (A15). Here $\widetilde{\beta}_f$ and $\widetilde{\beta}_m$ are chosen such that theory and experiment correlate for the thermal coefficients of expansion.

The ply shear moduli are given by

$$G_{\ell 12} = \frac{G_{m12}}{\dfrac{G_{m12}}{C_f'^2 G_{f12}} \overline{k}_f + \dfrac{\overline{k}_m}{C_m'^2}} \qquad (A17)$$

$$G_{\ell 13} = \frac{G_{m13}}{\dfrac{G_{m13}}{C_f'^2 G_{f13}} \overline{k}_f + \dfrac{\overline{k}_m}{C_m'^2}} \qquad (A18)$$

$$G_{\ell 23} = \frac{G_{m23}}{\dfrac{G_{m23}}{C_f''^2 G_{f23}} \overline{k}_f + \dfrac{\overline{k}_m}{C_m''^2}} \qquad (A19)$$

where

$$\left. \begin{aligned} C_f' &= \left(\frac{\overline{k}_f}{k_f}\right) \beta_f' \\[2em] C_m' &= \left(\frac{\overline{k}_m}{k_m}\right) \beta_m' \end{aligned} \right\} \qquad (A20)$$

$$\left. \begin{aligned} C_f'' &= \left(\frac{\overline{k}_f}{k_f}\right) \beta_f'' \\[2em] C_m'' &= \left(\frac{\overline{k}_m}{k_m}\right) \beta_m'' \end{aligned} \right\} \qquad (A21)$$

The parameters β_f', β_m', β_f'', and β_m'' are empirical factors and are to be chosen such that predicted and experimental results for the shear moduli correlate. The empirical

33

factors β'_f and β'_m can be selected from horizontal-shear-beam tests where the filaments are parallel to the beam axis. The empirical factors β''_f and β''_m can be selected from horizontal-shear-beam tests where the filaments are normal to the beam axis. It is noted that the condition

$$G_{l\,23} = \frac{E_{l\,33}}{2(1 + \nu_{l\,32})} = \frac{E_{l\,22}}{2(1 + \nu_{l\,23})} \tag{A22}$$

should be satisfied when the ply possesses transverse isotropy in the 2-3 plane. For this case,

$$\left.\begin{array}{c} E_{l\,33} = E_{l\,22} \\[2ex] \nu_{l\,32} = \nu_{l\,23} \end{array}\right\} \tag{A23}$$

The hydrostatic ply bulk modulus is given by

$$\frac{1}{K_l} = \left(\frac{1}{E_{l\,11}} + \frac{1}{E_{l\,22}} + \frac{1}{E_{l\,33}}\right) - 2\left(\frac{\nu_{l\,12}}{E_{l\,11}} + \frac{\nu_{l\,23}}{E_{l\,22}} + \frac{\nu_{l\,13}}{E_{l\,11}}\right) \tag{A24}$$

The ply heat capacity is given by

$$H_{cl} = \left(\frac{1}{\rho_l}\right)\left[H_{cf}\rho_f \bar{k}_f + H_{cm}\rho_m \bar{k}_m\right] \tag{A25}$$

where ρ_l is the ply weight density given by

$$\rho_l = \left[\rho_f \bar{k}_f + \rho_m \bar{k}_m\right] \tag{A26}$$

The heat conductivity of the matrix containing randomly distributed spherical voids is given by

$$\bar{K}_{m\alpha\alpha} = K_{m\alpha\alpha}\left[\frac{2\beta_{kv}K_{m\alpha\alpha} + K_v - 2k_v(K_{m\alpha\alpha} - K_v)}{2K_{m\alpha\alpha} + K_v - k_v(K_{m\alpha\alpha} - K_v)}\right] \tag{A27}$$

34

where K_v denotes the air conductivity and the parameter β_{kv} is the empirical factor chosen so that predicted and experimental results correlate. The subscripts $\alpha\alpha$ refer to the orthotropic axes of the matrix. The heat conductivities of the ply are given by

$$\left.\begin{aligned}
K_{l\,11} &= \beta_{k1}\overline{k}_f K_{f11} + k_m \overline{K}_{m11} \\[2em]
K_{l\,22} &= \overline{K}_{m22}\left[1 - \beta_{k2}\sqrt{k_f} + \cfrac{1}{\cfrac{1}{\beta_{k2}\sqrt{k_f}} - \left(1 - \cfrac{\overline{K}_{m22}}{K_{f22}}\right)}\right] \\[2em]
K_{l\,33} &= \overline{K}_{m33}\left[1 - \beta_{k3}\sqrt{k_f} + \cfrac{1}{\cfrac{1}{\beta_{k3}\sqrt{k_f}} - \left(1 - \cfrac{\overline{K}_{m33}}{K_{f33}}\right)}\right]
\end{aligned}\right\} \qquad \text{(A28)}$$

It is important to note that k_m is used in the first of equations (A28) instead of $\overline{k}_m$ since $\overline{K}_{m\alpha\alpha}$ includes the void effects. The parameters β_{k1}, etc. are semiempirical factors chosen so that predicted and experimental results correlate.

APPENDIX B

EQUATIONS FOR FAILURE STRESSES (STRENGTHS) AND TRANSFORMATION

Matrix-Strain Magnification Factors and Void Effects

The transverse and shear matrix-strain magnification factors (appendix of ref. 18 or ch. 2 of ref. 26) are

$$\varphi_{\mu 22} = \left[\frac{1}{1 + p(\overline{A} - 1)}\right]\left[1 + p(\nu_{f12} - \nu_{m12}\overline{A})\left(\frac{E_{l22}\sigma_{l11} - \nu_{l21}E_{l11}\sigma_{l22}}{E_{l11}\sigma_{l22} - \nu_{l12}E_{l22}\sigma_{l11}}\right)\right] \qquad \text{(B1)}$$

if $E_{l11}\sigma_{l22} - \nu_{l12}E_{l11} \neq 0$,

$$\varphi_{\mu 22} = 1 \qquad \text{(B2)}$$

if $E_{l11}\sigma_{l22} - \nu_{l12}E_{l22}\sigma_{l11} = 0$,

$$\varphi_{\mu 12} = \frac{1}{1 - p\left(1 - \dfrac{G_{m12}}{G_{f12}}\right)} \qquad \text{(B3)}$$

where

$$p = \left(\frac{4\overline{k}_f}{\pi}\right)^{1/2} \qquad \text{(B4)}$$

and

$$\overline{A} = \frac{1 - \nu_{f12}\nu_{f21}}{1 - \nu_{m12}\nu_{m21}}\left(\frac{E_{m22}}{E_{f22}}\right) \qquad \text{(B5)}$$

The maximum void effect factor is given by

$$\beta_{\mathrm{v}} = \frac{1}{1 - \left(\dfrac{4k_{\mathrm{v}}}{\pi k_{\mathrm{m}}}\right)^{1/2}} \tag{B6}$$

The parameters E, G, ν, and σ denote longitudinal modulus, shear modulus, Poisson ratio, and stress, respectively. The subscripts v, f, and m denote void, filament, and matrix, respectively, and the numerical subscripts correspond to the filament directions depicted in figure 1. The variable k_{v} is the void content, and $\bar{k}_{\mathrm{f}}$ and k_{m} are defined by equations (A1) and (A2), respectively.

Uniaxial Strengths

The uniaxial strengths $S_{l\,11T}$, $S_{l\,11C}$, $S_{l\,22T}$, $S_{l\,22C}$, and $S_{l\,12S}$ are given by (ref. 18)

$$S_{l\,11T} = S_{\mathrm{fT}}\left[\beta_{\mathrm{fT}}\bar{k}_{\mathrm{f}} + \beta_{\mathrm{mT}}\bar{k}_{\mathrm{m}}\left(\frac{E_{\mathrm{m}11}}{E_{\mathrm{f}11}}\right)\right] \tag{B7}$$

$$S_{l\,11C} = \min\left\{S_{\mathrm{mC}}\left[\beta_{\mathrm{mC}}\bar{k}_{\mathrm{m}} + \beta_{\mathrm{fC}}\bar{k}_{\mathrm{f}}\left(\frac{E_{\mathrm{f}11}}{E_{\mathrm{m}11}}\right)\right],\ (a_1 S_{l\,12S} + a_2)\right\} \tag{B8}$$

$$S_{l\,22T} = \beta_{22T}\frac{\epsilon_{\mathrm{mpT}}}{\beta_{\mathrm{v}}\varphi_{\mu 22}}E_{l\,22} \tag{B9}$$

$$S_{l\,22C} = \beta_{22C}\frac{\epsilon_{\mathrm{mpC}}}{\beta_{\mathrm{v}}\varphi_{\mu 22}}E_{l\,22} \tag{B10}$$

$$S_{l\,12S} = \beta_{12S}\frac{\epsilon_{\mathrm{mpS}}}{\beta_{\mathrm{v}}\varphi_{\mu 12}}G_{l\,12} \tag{B11}$$

where S_{fT}, S_{mC}, ϵ_{mpT}, ϵ_{mpC}, and ϵ_{mpS} represent filament bundle strength, matrix compressive strength, matrix tensile yield strain, matrix compressive yield strain, and matrix shear yield strain, respectively; E and G denote normal and shear moduli; k is the volume fraction, and φ_{μ} and β_{v} represent the strain magnification factors and

the maximum void effects, respectively; and the remaining β's denote the simple strength correlation coefficients.

Combined-Stress Strength Criterion

The ply failure criterion for combined stress is given by (ref. 18)

$$F(\sigma_l, S_l, K_{l\,12}) = 1 - \left[\left(\frac{\sigma_{l\,11\alpha}}{S_{l\,11\alpha}}\right)^2 + \left(\frac{\sigma_{l\,22\beta}}{S_{l\,22\beta}}\right)^2 + \left(\frac{\sigma_{l\,12S}}{S_{l\,12S}}\right)^2 - K'_{l\,12\alpha\beta}K_{l\,12}\frac{\sigma_{l\,11\alpha}\sigma_{l\,22\beta}}{|S_{l\,11\alpha}||S_{l\,22\beta}|}\right]$$

(B12)

where F denotes the combined-stress strength criterion as follows:

$$F(\sigma_l, S_l, K_{l\,12}) > 0 \qquad \text{no failure}$$

$$F(\sigma_l, S_l, K_{l\,12}) = 0 \qquad \text{onset of failure}$$

$$F(\sigma_l, S_l, K_{l\,12}) < 0 \qquad \text{failure condition exceeded}$$

and where subscripts α and β denote T (tension) or C (compression), σ_l the applied stress state determined from the stress analysis, S the unidirectional filamentary composite (UFC) simple strength either determined from the equations described previously or measured experimentally, and $K'_{l\,12\alpha\beta}$ the theory-experiment correlation coefficient determined as described in reference 18. The coefficient $K_{l\,12}$ is given by

$$K_{l\,12} = \frac{(1 + 4\nu_{l\,12} - \nu_{l\,13})E_{l\,22} + (1 - \nu_{l\,23})E_{l\,11}}{\left[E_{l\,11}E_{l\,22}(2 + \nu_{l\,12} + \nu_{l\,13})(2 + \nu_{l\,21} + \nu_{l\,23})\right]^{1/2}}$$

(B13)

where E_l and ν_l denote UFC modulus and Poisson's ratio, respectively. The subscripts 11, 13, etc. refer to the corresponding axes in figure 1. For the case of isotropic material, equation (B13) reduces to one, as can be verified by direct substitution, and equation (B12) reduces to the well known von Mises criterion.

Off-axis failure envelopes for UFC. - There are four possible off-axis loadings on a ply - namely, normal tensile force, normal compressive force, positive shear force, and negative shear force (ref. 18). The corresponding equations are, respectively,

$$S_{\ell xx\alpha} = \cfrac{1}{\left[\cfrac{\cos^4\theta}{S_{\ell 11\alpha}^2} + \cfrac{\sin^4\theta}{S_{\ell 22\alpha}^2} + \cfrac{1}{4}\left(\cfrac{1}{S_{\ell 12S}^2} - \cfrac{K'_{\ell 12\alpha\alpha}k_{\ell 12}}{\left|S_{\ell 11\alpha}\right|\left|S_{\ell 22\alpha}\right|}\right)\sin^2 2\theta\right]^{1/2}} \qquad \text{(B14)}$$

$$S_{\ell xy\alpha\beta} = \cfrac{1}{\left[\left(\cfrac{1}{S_{\ell 11\alpha}^2} + \cfrac{1}{S_{\ell 22\beta}^2} + \cfrac{K'_{\ell 12\alpha\beta}K_{\ell 12}}{\left|S_{\ell 11\alpha}\right|\left|S_{\ell 22\beta}\right|}\right)\sin^2 2\theta + \cfrac{\cos^2 2\theta}{S_{\ell 12S}^2}\right]^{1/2}} \qquad \text{(B15)}$$

where S_ℓ is the failure strength, θ the angle between filament and load directions, and α either T (tension-tensile load envelope) or C (compression-compressive load envelope). When $\alpha = T$ and $\beta = C$, equation (B15) describes the positive shear envelope; when $\alpha = C$ and $\beta = T$, equation (B15) describes the negative shear envelope.

Transformation Equations for Off-Axis UFC

The two-dimensional elastic and thermal constants of off-axis UFC are given by (refs. 23 and 24)

$$[E_{cx}]^{-1} = [R_\ell]^T [E_\ell]^{-1} [R_\ell] \qquad \text{(B16)}$$

$$\{\alpha_{cx}\} = [R_\ell]\{\alpha_\ell\} \qquad \text{(B17)}$$

where

$$[R_\ell] = \begin{bmatrix} \cos^2\theta & \sin^2\theta & \dfrac{1}{2}\sin 2\theta \\[2ex] \sin^2\theta & \cos^2\theta & -\dfrac{1}{2}\sin 2\theta \\[2ex] -\sin 2\theta & \sin 2\theta & \cos 2\theta \end{bmatrix} \qquad \text{(B18)}$$

$$[E_l] = \begin{bmatrix} \dfrac{1}{E_{l\,11}} & -\dfrac{\nu_{l\,21}}{E_{l\,22}} & 0 \\[2ex] -\dfrac{\nu_{l\,12}}{E_{l\,11}} & \dfrac{1}{E_{l\,22}} & 0 \\[2ex] 0 & 0 & \dfrac{1}{G_{l\,12}} \end{bmatrix} \tag{B19}$$

$$\{\alpha_l\} = \left\{ \begin{array}{c} \alpha_{l\,11} \\ \alpha_{l\,22} \\ 0 \end{array} \right\} \tag{B20}$$

and where θ is the angle between the x-axis and the fiber direction. The elements in $[E_{cx}]$ and $\{\alpha_{cx}\}$ are obtained by replacing l by cx in equations (B19) and (B20).

Equations for Angle-Ply Composites

Let z_{ti} and z_{bi} represent distances from some reference plane to the top and bottom of the ith ply, respectively. Then, neglecting interply layer contributions, the elastic and thermal coefficients of expansion of angle-ply composites are given by, respectively,

$$[E_{cx}]^{-1} = \frac{1}{t_c} \sum_{i=1}^{N_l} (z_{ti} - z_{bi})[R_{l\,i}]^T [E_{l\,i}]^{-1} [R_{l\,i}] \tag{B21}$$

$$\{\alpha_{cx}\} = [E_{cx}] \sum_{i=1}^{N_l} [R_{l\,i}]^T [E_{l\,i}]^{-1} \{\alpha_{l\,i}\} \tag{B22}$$

$$t_c = \sum_{i=1}^{N_l} t_{l\,i} \tag{B23}$$

where $[R_{\ell i}]$, $[E_{\ell i}]$, and $\{\alpha_{\ell i}\}$ are matrices representing transformation (eq. (B18)), elastic constants (eq. (B19)), and thermal coefficients of expansion (eq. (B20)) for the ith ply, respectively.

REFERENCES

1. Kelly, A.; and Davies, G. J.: The Principles of the Fiber Reinforcement of Metals. Metallurg. Rev., vol. 10, no. 37, 1965, pp. 1-78.

2. Weeton, John W.; and Signorelli, Robert A.: Fiber-Metal Composite Materials. NASA TN D-3530, 1966.

3. Alexander, John A.; Shaver, Robert G.; and Withers, James C.: Critical Analysis of Accumulated Experimental Data on Filament-Reinforced Metal Matrix Composites. General Technologies Corp. (NASA CR-106490), June 1969.

4. Karpinos, D. M.; and Tuchinskii, L. I.: Fiber Reinforced Metals (FRM) (A Review of Literature). Poroshkovaia Met., vol. 8, July 1968, pp. 37-48.

5. Weeton, John W.: Fiber-Metal Matrix Composites. Machine Design, vol. 41, no. 4, Feb. 20, 1969, pp. 142-156.

6. Niese, D. E.; Fleck, J. N.; Kistler, C. W., Jr.; and Machlin, I.: Carbon-Filament-Reinforced Cobalt and Nickel. Paper 68-338, AIAA, Apr. 1968.

7. Toy, Albert: Mechanical Properties of Beryllium Filament-Reinforced Aluminum Composites. J. Materials, vol. 3, no. 1, Mar. 1968, pp. 43-58.

8. Petrasek, D. W.; and Signorelli, R. A.: Tungsten Alloy Fiber Reinforced Nickel Base Alloy Composites for High Temperature Turbojet Engine Applications. Presented at the ASTM Symposium on Composite Materials Testing and Design, New Orleans, La., Feb. 10-14, 1969.

9. Anon.: Composite Materials: Testing and Design. Spec. Tech. Publ. 460, ASTM, 1969.

10. Metcalfe, A. G.; and Schmitz, G. K.: Current Status of Titanium-Boron Composites for Gas Turbines. Paper 69-GT-1, ASME, Mar. 1969.

11. Sara, R. B.: Fabrication and Properties of Graphite Fiber, Nickel-Matrix Composite. Science of Advanced Materials and Process Engineering Proceedings. Vol. 14. Western Periodicals Co., 1968, paper II-4A-4.

12. Davis, L. W.: Characterization of Metal Matrix Composites. Paper 69-GT-23, ASME, Mar. 1969.

13. Jackson, Peter W.: Some Studies of the Compatibility of Graphite and Other Fibers with Metal Matrices. Paper W-9-20.1, ASM, Mar. 1969.

14. Metzger, G. E.: Welding of Metal-Matrix Fiber-Reinforced Materials. Paper W-9-23.2, ASM, Mar. 1969.

15. Mangiapane, J. A.; Sattar, S. A.; Gray, D. F.; and Timoshenko, J. A.: Blading for Gas-Turbine Engines. J. Aircraft, vol. 6, no. 4, July-Aug. 1969, pp. 318-325.

16. Chamis, C. C.; and Sendeckyj, G. P.: Critique on Theories Predicting Thermoelastic Properties of Fibrous Composites. J. Composite Mat., vol. 2, no. 3, July 1968, pp. 332-358.

17. Chamis, C. C.: Thermoelastic Properties of Unidirectional Filamentary Composites by a Semiempirical Micromechanics Theory. Science of Advanced Materials and Process Engineering Proceedings. Vol. 14. Western Periodicals Co., 1968, paper I-4-5.

18. Chamis, Christos C.: Failure Criteria for Filamentary Composites. NASA TN D-5367, 1969.

19. Chen, P. E.; and Lin, J. M.: Transverse Properties of Fibrous Composites. Mat. Res. Standards, vol. 9, no. 8, Aug. 1969, pp. 29-33.

20. Antony, K. C.; and Chang, W. H.: Mechanical Properties of Al-B Composites. Trans. ASM, vol. 61, no. 3, Sept. 1968, pp. 550-558.

21. Chamis, C. C.: Important Factors in Fiber Composite Design. Proceedings of the 24th Annual Conference Society of the Plastics Industry, 1969, pp. 18-E-1 to 18-E-13.

22. Anon.: Advanced Composites Status Report. Conference Sponsored by the Air Force Materials Laboratory, Advanced Composites Division, hosted by Lockheed-Georgia, Sept. 25-26, 1968.

23. Lekhnitskii, S. G.: Theory of Elasticity of an Anisotropic Elastic Body. Holden-Day, Inc., 1963.

24. Anon.: Structural Design Guide for Advanced Composite Applications. North American Rockwell Corp., Aug. 1969. (Contract F33615-69-C-1368.)

25. Ashton, J. E.; Halpin, J. C.; and Petit, P. H.: Primer on Composite Materials: Analysis. Technomic Publ. Co., 1969.

26. Chamis, Christos C.: Design Oriented Analysis and Synthesis of Multilayered-Filamentary Structural Panels. Ph.D. Thesis, Case Western Reserve Univ., 1967, Ch. 4.

27. Chamis, Christos C.: Buckling of Anisotropic Composite Plates. Journal of the Structural Division, ASCE, Vol. 95, No. ST10, Oct. 1969, pp. 2119-2139.

28. Anon.: Fiber-Strengthened Metallic Composites. Spec. Tech. Publ. 427, ASTM, 1967.

29. Anon.: Metal Matrix Composites. Spec. Tech. Publ. 438, ASTM, 1968.

30. Anon.: Interfaces in Composites. Spec. Tech. Publ. 452, ASTM, 1969.

31. Mullin, J.; Berry, J. M.; and Gatti, A.: Some Fundamental Fracture Mechanisms Applicable to Advanced Filament Reinforced Composites. J. Composite Mat., vol. 2, no. 1, Jan. 1968, pp. 82-103.

32. Outwater, J. O.; and Murphy, M. C.: On the Fracture Energy of Unidirectional Laminates. Proceedings of the 24th Annual Conference Society of the Plastics Industry, 1969, pp. 11-C-1 to 11-C-8.

33. Holister, G. S.; and Thomas, C.: Fibre Reinforced Materials. Elsevier Publ. Co., 1966.

34. Broutman, L. J.; and Krock, R. H.: Modern Composite Materials. Addison-Wesley Publ. Co., 1967.

35. Anon.: Metal-Matrix Composites. Rep. DMIC Memo-243, Battelle Memorial Inst., May 1969.

36. Hanby, K. R.: Fiber-Reinforced Metal-Matrix Composites - 1968. Rep. DMIC-S-27, Battelle Memorial Institute, July 1, 1969. (Available from DDC or AD-858351.)

FIRST CLASS MAIL
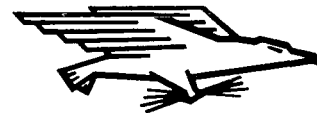
JIU 031 4/   51 ...

\I F IRCE ... ... LA: ...

KIRTI \ ... ...

' T t, ...

.IASTER: If Undeliverable (Section 158
           Postal Manual) Do Not Return

"The aeronautical and space activities of the United States shall be conducted so as to contribute . . . to the expansion of human knowledge of phenomena in the atmosphere and space. The Administration shall provide for the widest practicable and appropriate dissemination of information concerning its activities and the results thereof."

— NATIONAL AERONAUTICS AND SPACE ACT OF 1958

NASA SCIENTIFIC AND TECHNICAL PUBLICATIONS

TECHNICAL REPORTS: Scientific and technical information considered important, complete, and a lasting contribution to existing knowledge.

TECHNICAL NOTES: Information less broad in scope but nevertheless of importance as a contribution to existing knowledge.

TECHNICAL MEMORANDUMS: Information receiving limited distribution because of preliminary data, security classification, or other reasons.

CONTRACTOR REPORTS: Scientific and technical information generated under a NASA contract or grant and considered an important contribution to existing knowledge.

TECHNICAL TRANSLATIONS: Information published in a foreign language considered to merit NASA distribution in English.

SPECIAL PUBLICATIONS: Information derived from or of value to NASA activities. Publications include conference proceedings, monographs, data compilations, handbooks, sourcebooks, and special bibliographies.

TECHNOLOGY UTILIZATION PUBLICATIONS: Information on technology used by NASA that may be of particular interest in commercial and other non-aerospace applications. Publications include Tech Briefs, Technology Utilization Reports and Notes, and Technology Surveys.

Details on the availability of these publications may be obtained from:

SCIENTIFIC AND TECHNICAL INFORMATION DIVISION

NATIONAL AERONAUTICS AND SPACE ADMINISTRATION
Washington, D.C. 20546